RESEARCH PAPER

CrossMark

Adaptive gradient-enhanced kriging model for variable-stiffness composite panels using Isogeometric analysis

Peng Hao[1] · Shaojun Feng[1] · Ke Zhang[1] · Zheng Li[1] · Bo Wang[1] · Gang Li[1]

Abstract

Variable-stiffness panel is very promising for the cutout reinforcement of composite structures. However, due to the increase of design variables, the optimization of variable-stiffness panels becomes very challenging, even if surrogate model is utilized, because the fidelity of surrogate model is difficult to guarantee for high-dimensional problems. In this study, isogeometric analysis method (IGA) is employed to predict the buckling load of variable-stiffness panels, which can produce accurate prediction with less computational cost compared to traditional FEA, moreover, it can provide analytical sensitivity for optimization. On this basis, an adaptive gradient-enhanced kriging (GEK) model assisted by a novel multiple points infilling criterion is constructed for the global optimization of variable-stiffness composite panels. The proposed method is compared with traditional surrogate model, and results show that the proposed method can find a better optimum design in a more efficient manner. It can be concluded that the proposed method is able to fully explore the advantages of IGA including exact modelling, analysis and analytical sensitivity, which is particularly suitable for the design of variable-stiffness panels and other complex structures.

Keywords Variable-stiffness panels · Buckling · Fiber path · Optimization · Adaptive gradient-enhanced kriging model · Multiple points infilling

1 Introduction

For aircraft and aerospace structures, composite material has been increasingly used in the load-carrying components (Wang et al. 2002; Zhu et al. 2016). Due to the limitation of traditional manufacturing process, straight fiber paths are commonly utilized in the practical design of aircraft and aerospace structures, like fuselage, rocket interstage, fuel tank, etc. Buckling is the main failure consideration for thin-walled structures under axial or other combined loads (Bourada et al. 2016; Hao et al. 2016b; Wang et al. 2014; Hao et al. 2017b). The buckling behavior is highly dependent on stacking sequences for composite structures, and thus many studies were devoted to the stacking sequence optimization for maximum buckling load. In general, due to the inherent feature of multiple local optima, heuristic methods were employed to find the global optimum (Le and Haftka 1993; Soremekun et al. 2001; Liu et al. 2000; Karakaya and Soykasap 2009). Blending constraint (Liu et al. 2011; Kristinsdottir et al. 2001), patch constraint (Zehnder and Emanni 2006) and other manufacturing constraints (Wang and Costin 1992; Sørensen and Lund 2013) were considered for ease of manufacturing. Because the buckling analysis of thin-walled structures is time-consuming, surrogate model has been adopted in order to release the high computational burden (Rikards et al. 2004; Abouhamze and Shakeri 2007).

As a promising structural concept, variable-stiffness composite panels with curvilinear fiber path can tailor the in-plane stiffness for improving the loading path and stress distribution. According to the previous studies (Van den Brink et al. 2012; Gürdal et al. 2008), an improvement of buckling load ranging from 35% to 67% can be achieved by using a variable-stiffness design compared to traditional constant-stiffness design with straight fiber path, and this can be attributed to the redistribution of in-plane loads from critical regions to

---

Responsible Editor: Hai Huang

✉ Peng Hao
  haopeng@dlut.edu.cn

✉ Bo Wang
  wangbo@dlut.edu.cn

[1] State Key Laboratory of Structural Analysis for Industrial Equipment, Department of Engineering Mechanics, Dalian University of Technology, Dalian 116023, China

relatively stiff regions. Due to this advantage, the design and optimization of variable-stiffness panels have attracted much attention in recent years (Madeo et al. 2017; Wu et al. 2015; Peeters et al. 2015; Rouhi et al. 2017). To start with, several representation functions of curvilinear fiber path were developed, including linear variation function (Gürdal et al. 2008), quadratic and cubical functions (Muc and Ulatowska 2010), trigonometric function (Blom et al. 2009), etc. For these methods, a reference path is defined firstly, and then a shifting criterion is specified, finally, the fiber angle in arbitrary region can be expressed explicitly. In general, linear variation function is the simplest method to describe the fiber path, in which only two design variables are involved, and thus it has been extensively investigated in the previous studies. However, the design space of variable-stiffness panels is also highly restricted for this rough representation. Besides, level set method was also used to represent a series of continuous equally spaced fiber paths, and an optimization for the minimal compliance was performed to find the optimum fiber path (Brampton et al. 2015). In addition, a specific scalar function corresponding to the cocurrent and equipotential lines in the flow field was used to define a set of fiber angles within one ply (Niu et al. 2016), and the fiber path can be guaranteed to be continuous and non-intersect. Moreover, since a pair of cocurrent and equipotential lines passing through arbitrary point are orthogonal to each other, the other function can be determined if one is defined, which means that the fiber paths of two adjacent plies can be obtained simultaneously. Based on these representation methods, the optimization of variable-stiffness panels can be carried out. Obviously, for the design of variable-stiffness panels, the total number of design variables would be very large, even if linear variation function is used. Assuming that n_r is the number of design variables for each ply, the total number of design variables would be $N_t = n_r \times n_p$, where n_p is the number of independent ply. For high-dimension optimization problems, a multi-step framework was established by Rouhi et al. (2017), and its basic idea is to narrow the design space according to the optimum results in previous steps. Jing et al. (2015) proposed a global shared-layer blending method for solving the tailoring problem of tapered composite structure, which can successfully avoid delamination at ply-drop location and generate manufacturable structures with maximum blending property. Considering multiple manufacturing constraints, Jing et al. (2016) further developed a multi-level optimization framework based on a sequential permutation table method, and a high design efficiency is achieved compared to traditional methods. For curvilinear fiber path, several specific manufacturing constraints were also considered in the optimization process, such as curvature constraint, parallelism constraint (Lozano et al. 2016; Montemurro and Catapano 2017).

As a type of promising numerical method for structural analysis, IGA proposed by Hughes et al. (2005) can provide exact modeling of structures with complex geometry and boundary condition, by which CAD and CAE can be integrated together due to the utilization of smooth spline basis functions. Compared to traditional FEA, IGA can produce accurate solution with less computational cost, because only less degree of freedom is required for the IGA to achieve similar accuracy. More importantly, IGA can provide analytical sensitivity expression, which is particularly suitable for the optimization of variable-stiffness panels.

Due to the complex characteristic of curvilinear fiber path, the optimization of variable-stiffness panels is still very challenging, because the design space is highly nonconvex, which results in the fact that traditional gradient-based optimization methods may trapped into local optima. In this case, heuristic methods can guarantee the global optimization capacity but is computationally inefficient. Surrogate model is a powerful tool for the global optimization of complex problems with relatively small computational cost (Hao et al. 2012, 2013). A detailed comparison of different surrogate models was reported by Nik et al. (2014) for the optimum design of variable-stiffness composite panels. Due to the inherent multi-local-optima feature, the fidelity of surrogate model is difficult to ensure, even if a large number of training samples are used. In order to improve the prediction accuracy of surrogate model, there have been plenty of related studies on the construction and dynamic updating of surrogate model. It has been demonstrated that adding one single point at a time may not be efficient when the main concern is wall-clock time (rather than number of simulations) and simulations can run in parallel (Viana et al. 2013). Thus, various multiple points infilling criterions have been developed, and the most famous one is known as Efficient Global Optimization (EGO) method (Jones et al. 1998), where the expected improvement (EI) is used to balance the prediction uncertainty and objective value. Then, many improved algorithms were developed to balance the exploration and exploitation, including the weighted EI (Sóbester et al. 2005), generalized EI (Sasena et al. 2002), augmented EI (Huang et al. 2006), modified EI (Rehman et al. 2014). The EGO method was adopted in the optimization of stiffened composite panels (Haftka et al. 2016), and a feasible optimal structure was obtained with a low computational cost (Todoroki and Sekishiro 2008). Recently, Li et al. (2016) proposed an expected improvement and mutual information (EI&MI) infilling criterion, which employs the entropy to precisely quantify the uncertainty of surrogate model, and then balances the global exploration and local exploitation when adding new samples.

For traditional surrogate model, only exact function values of design points are used to establish the surrogate model, thus plenty of sampling points must be calculated in the design of

experiment to guarantee the approximation quality of surrogate model. However, additional information such as gradient/sensitivity is not fully utilized (Han and Görtz 2012), whereas it can be obtained analytically for the IGA. In order to improve the prediction accuracy of surrogate model, and also reduce the number of required sampling points, gradient-enhanced Kriging (GEK) model was developed to incorporate gradient or sensitivity information into the construction of surrogate model (Chung and Alonso 2002; Yamazaki et al. 2010; Yamazaki and Mavriplis 2013; Ulaganathan et al. 2015), including direct GEK and indirect GEK, respectively (Chung and Alonso 2002). For the direct GEK developed by Morris et al. (1993), gradient/sensitivity information is directly used to establish Kriging model by expanding the correlation function and correlation vector. Laurent et al. (2013) compared the direct GEK and Kriging model by mechanical functions, and it is found that the direct GEK can lead to a significant decrease in the number of required sample points. This is due to the fact that, additional points in the vicinity of real sample points with small distance, are approximated by using the gradient information. Unlike the direct GEK, the indirect GEK employs the same correlation function as the one of Kriging, and the samples include the real sample points and additional points. According to the works by Laurenceau and Sagaut (2008), the direct and indirect GEK show a same fitting accuracy with identical parameters, when the step size is small enough, though it is difficult to be determined. Moreover, (Yamazaki et al. 2010; Yamazaki and Mavriplis 2013) developed a gradient/Hessian-enhanced Kriging (HGEK) model using the second-order gradient information, which is particularly suitable for high-dimensional complex problems. It can be expected that once the GEK model is combined with IGA, the optimization efficiency of variable-stiffness panels would be improved significantly, because the advantages of exact modelling, analysis and analytical sensitivity can be fully explored.

In this study, an efficient optimization framework is developed for the design of variable-stiffness panels by combination of IGA method, GEK method and multiple points infilling criterion. This paper is organized as follows. In Section 2, the basic formulas of isogeometric buckling analysis for variable-stiffness panels is introduced. In Section 3, gradient-enhanced kriging model is presented, and a new multiple points infilling criterion is developed based on EI&MI, i.e. expected improvement with Gauss distance (EIGD). In Section 4, an optimization framework is proposed for the design of variable-stiffness panels based on GEK. In Section 5, the proposed method is compared with several existing optimization methods. Finally, conclusions are drawn, and results show that the proposed method can find a better optimum design in a more efficient manner, which can significantly improve the computational efficiency of variable-stiffness panels for aerospace industry.

2 Sensitivity derivation based on isogeometric analysis

For the linear buckling analysis of variable-stiffness panels, the governing equation can be expressed as

$$(\mathbf{K} - \lambda \mathbf{K}_G)\mathbf{a}^i = 0 \qquad i = 1, 2, \ldots, r \tag{1}$$

where $\mathbf{K}$ is the global stiffness matrix, $\mathbf{K_G}$ is the geometric matrix. λ is the buckling factor, and the buckling load can be obtained by multiplying the buckling factor with the predefined load. $\mathbf{a}^i$ is the ith buckling mode, and r is the total number of degrees of freedom.

During the optimization process, the buckling factor λ (usually defined as optimization objective) will change due to the variation of design variables a, and the change of design variables a is summed up to the sensitivity. The main process of the sensitivity derivation is given herein. The derivative of the objective function λ with respect to the design variable a can be expressed as

$$\frac{\partial \lambda}{\partial a} = \frac{1}{\mathbf{d}^T \mathbf{K}_G \mathbf{d}} \left[\mathbf{d}^T \frac{\partial \mathbf{K}}{\partial a} \mathbf{d} - \lambda \mathbf{d}^T \frac{\partial \mathbf{K}_G}{\partial a} \mathbf{d} \right] \tag{2}$$

where $\mathbf{d}$ is the instability waveform.

As is evident from (2), $\frac{\partial \mathbf{K}}{\partial a}$ and $\frac{\partial \mathbf{K}_G}{\partial a}$ should be obtained. The global stiffness matrix $\mathbf{K}$ can be expressed as

$$\mathbf{K} = \sum_{n=1}^{numele} \mathbf{k}_n \tag{3}$$

where $\mathbf{k}_n$ is the element stiffness matrix, and $numele$ represents the element number. The element stiffness matrix can be calculated through the loop in Gaussian points

$$\mathbf{k}_n = \sum_{m=1}^{numgas} \mathbf{B}^T \overline{\mathbf{Q}} \mathbf{B} w_1 w_2 |\mathbf{J}| \tag{4}$$

where $\mathbf{B}$ is the strain matrix, w_1 and w_2 are two weighted coefficients. $|\mathbf{J}|$ denotes the Jacobian matric, $\overline{\mathbf{Q}}$ is the global plane-stress stiffness, $numgas$ represents the number of Gaussian points. Similarly, the geometric stiffness matrix can also be obtained through the loop in Gaussian points

$$\mathbf{k}_{gn} = \sum_{m=1}^{numgas} \mathbf{G}^T [\sigma] \mathbf{G} h w_1 w_2 |\mathbf{J}| \tag{5}$$

where $[\sigma]$ is the initial stress matrix, $\mathbf{G}$ is the derivative matrix of shape function, and h is the lamination thickness.

$$\frac{\partial \mathbf{k}_{gn}}{\partial a} = \sum_{m=1}^{numgas} \mathbf{G}^T \frac{\partial [\sigma]}{\partial a} \mathbf{G} h w_1 w_2 |\mathbf{J}| \tag{6}$$

where

$$\boldsymbol{\sigma} = \mathbf{DB}\mathbf{u}^e \tag{7}$$

in which $\mathbf{D}$ is the material elastic matrix, $\mathbf{u}^e$ is the nodal displacement. In this case, the derivation only needs to concern about $[\sigma]$. According to the chain rule, $\frac{\partial\sigma}{\partial a}$ can be rewritten as

$$\frac{\partial\boldsymbol{\sigma}}{\partial a} = \frac{\partial\mathbf{D}}{\partial a}\mathbf{B}\mathbf{u}^e + \mathbf{DB}\frac{\partial\mathbf{u}^e}{\partial a} \tag{8}$$

3 Gradient-enhanced kriging model assisted by multiple points infilling criterion

3.1 Gradient-enhanced kriging model

In essence, the Kriging model is a statistical prediction method containing two components

$$Y(\boldsymbol{x}) = \beta + Z(\boldsymbol{x}) \tag{9}$$

where β is the regression coefficient, $Z(\boldsymbol{x})$ is the stochastic process with a mean of zero and a variance of σ^2.

Kriging model can predict the response values in arbitrary design space by the following equation

$$\hat{y}(x) = \beta + \boldsymbol{r}_{(\boldsymbol{x})}^T\boldsymbol{R}^{-1}(\boldsymbol{Y}-\beta\boldsymbol{F}) \tag{10}$$

where $\boldsymbol{Y}$ is the column vector of response data of known design samples, $\boldsymbol{R}$ is the matrix of correlation function specified by user, $\boldsymbol{r}$ is the correlation vector, $\boldsymbol{F}$ is the regression vector, which is a unit matrix for constant regression.

For the indirect GEK (Liu and Batill 2002), gradient information is used to calculate additional points by the first-order Taylor approximation as

$$\begin{aligned} \boldsymbol{x}_{add}^i &= \boldsymbol{x}^i + \Delta\boldsymbol{x} \\ \boldsymbol{y}(\boldsymbol{x}_{add}^i) &= \boldsymbol{y}(\boldsymbol{x}^i) + \Delta\boldsymbol{x}^T\left[\frac{\partial y(\boldsymbol{x}^i)}{\partial\boldsymbol{x}}\right] \end{aligned} \tag{11}$$

In the direct GEK, the gradient information is used to establish the matrix of $\boldsymbol{R}$. The matrix of samples and values are

$$\begin{aligned} S &= \left[\boldsymbol{x}^1, \boldsymbol{x}^2, \cdots, \boldsymbol{x}^n, \boldsymbol{x}^1\cdots\boldsymbol{x}^1, \boldsymbol{x}^2\cdots\boldsymbol{x}^2, \cdots, \boldsymbol{x}^n\cdots\boldsymbol{x}^n\right]^T \in \mathfrak{R}^{(n+n\times dim)\times dim} \\ Y &= \left[y(\boldsymbol{x}^1)\cdots y(\boldsymbol{x}^n), \frac{\partial y(\boldsymbol{x}^1)}{x_1^1}\cdots\frac{\partial y(\boldsymbol{x}^1)}{x_d^1}, \cdots, \frac{\partial y(\boldsymbol{x}^n)}{x_1^n}\cdots\frac{\partial y(\boldsymbol{x}^n)}{x_{dim}^n}\right]^T \in \mathfrak{R}^{n+n\times dim} \end{aligned} \tag{12}$$

where n denotes the number of samples, dim is the number of dimensions. The detailed derivation process of $\boldsymbol{R}$ and $\boldsymbol{r}$ can be found in the Appendix.

$$\begin{aligned} \hat{y}(x) &= \beta + \boldsymbol{r}_{(\boldsymbol{x})}^T\boldsymbol{R}^{-1}(\boldsymbol{Y}-\beta\boldsymbol{F}) \\ \beta &= \left(\boldsymbol{F}^T\boldsymbol{R}^{-1}\boldsymbol{F}\right)^{-1}\boldsymbol{F}^T\boldsymbol{R}^{-1}\boldsymbol{Y} \end{aligned} \tag{13}$$

It should be noted that there is no additional sample point, thus the matrix calculation is much better. In this paper, the direct GEK is utilized.

3.2 EI&MI multiple points infilling criterion

In order to fully explore the design space, some infilling criterions are used to search for new samples and then update the surrogate model, until convergence is achieved. The infilling criterions can be divided into single point criterion and multiple points criterion. As an important improvement of EI criterion, a multiple points infilling criterion named EI&MI was developed by Li et al. (2016). The EI&MI adopts the entropy to precisely measure the uncertainty of Kriging model, and then balances the global exploration and local exploitation of multiple points infilling sampling criteria. Only the key process of EI&MI is introduced herein, and the detail information can be found in Ref. (Li et al. 2016).

In any given step-loop, $S \subset \Omega$ denotes the evaluated design points. According to the principle of maximum entropy, the global exploration of infilled samples should be achieved as follows
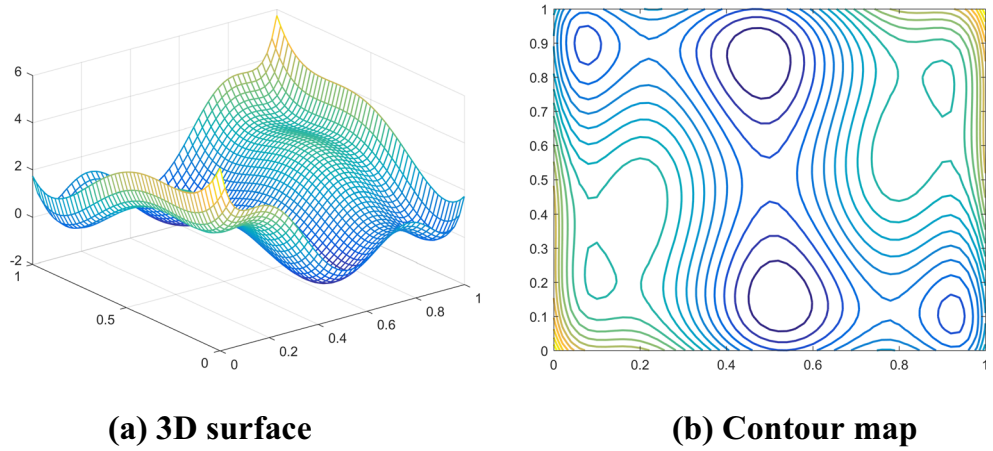
$$\begin{aligned} H(&\mathbf{Y_X}|\mathbf{Y_S} = \mathbf{Y}) \\ &= -\int p(\mathbf{Y_X}|\mathbf{Y_S} = \mathbf{Y})\ln\left[\int p(\mathbf{Y_X}|\mathbf{Y_S} = \mathbf{Y})\right]d\mathbf{Y_X} \end{aligned} \tag{14}$$

Table 1 Typical kernel functions

Function	Expression
EXP	$\exp(-\alpha_k|d_k|)$
GAUSS	$\exp(-\alpha_k|d_k|^2)$
LIN	$\max\{0, 1-\alpha_k|d_k|\}$
SPLINE	$\varsigma(\xi_k) = \begin{cases} 1-15\xi_k^2 + 30\xi_k^3 & 0\leq\xi_k\leq 0.2 \\ 1.25(1-\xi_k)^3 & 0.2\leq\xi_k\leq 1, \xi_k = \alpha_k|d_k| \\ 0 & \xi_k\geq 1 \end{cases}$

Note that d_k is the distance between two points

(a) 3D surface

(b) Contour map

For the parallel points added, in order to avoid the high dimensional infilling criterion, we suggest to select the infilled samples one by one. Assuming that the number of selected infilled samples is $k-1$, the kth sample can be selected by

Find $\mathbf{x}_k$
Maximize $H(\mathbf{Y}_{\mathbf{X}_k}|\mathbf{Y}_{\mathbf{S}} = \mathbf{Y})$ (15)
Subject to : $\mathbf{x}_k \in \Omega$

where $\mathbf{x}_k$ denotes the kth infilled sample. Here, we would like to balance the two objectives in (15) into one function. The new function should maintain the good searching ability of the serial infilling criterion such as EI. Thus, $H(\mathbf{Y}_{\mathbf{X}_k}|\mathbf{Y}_{\mathbf{S}} = \mathbf{Y})$ is decomposed as

$$H(\mathbf{Y}_{\mathbf{X}_{k-1}}|\mathbf{Y}_{\mathbf{S}} = \mathbf{Y})$$
$$+ H(y(\mathbf{x}_k)|\mathbf{Y}_{\mathbf{S}} = \mathbf{Y}) - \text{MI}(\mathbf{Y}_{\mathbf{X}_{k-1}}, y(\mathbf{x}_k)|\mathbf{Y}_{\mathbf{S}} = \mathbf{Y}) \quad (16)$$

where MI is the mutual information. Consequently, the multiple points infilling criterion of EI&MI is obtained

Find $\mathbf{x}_k$
Maximize $\text{EIMI}(\mathbf{x}_k) = E[I(\mathbf{x}_k)]\exp\{-\rho\text{MI}[\mathbf{Y}_{\mathbf{X}_{k-1}}, y(\mathbf{x}_k)|\mathbf{Y}_{\mathbf{S}} = \mathbf{Y}]\}$
                          $\Rightarrow E[I(\mathbf{x}_k)]M^\rho(\mathbf{x}_k, \mathbf{X}_{k-1})$
Subject to : $\mathbf{x}_k \in \Omega$

$$\quad (17)$$

where

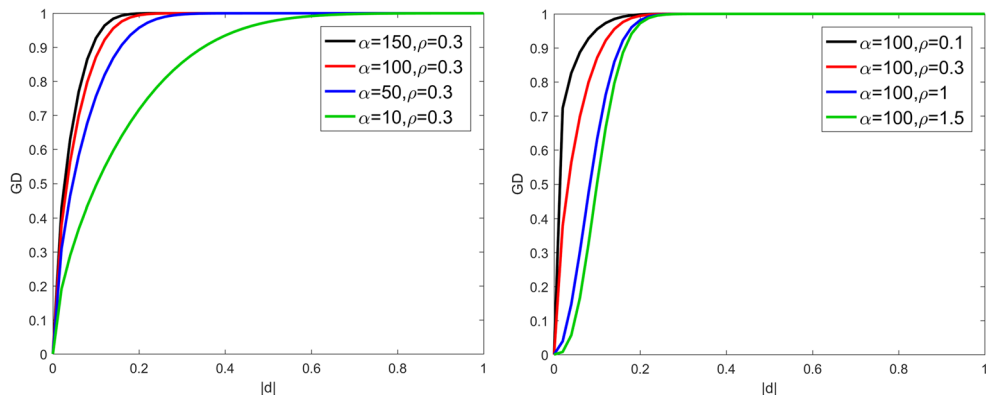$$M(\mathbf{x}_k, \mathbf{X}_{k-1}) = 1 - \hat{\mathbf{R}}_{x_k X_{k-1}} \hat{\mathbf{R}}^{-1}_{X_{k-1} X_{k-1}} \hat{\mathbf{R}}_{X_{k-1} x_k} \quad (18)$$

The range of M is $0 \le M(\mathbf{x}_k, \mathbf{X}_{k-1}) \le 1$. $M(\mathbf{x}_k, \mathbf{X}_{k-1}) = 0$ when $\mathbf{x}_k \in X_{k-1}$, and $M(\mathbf{x}_k, \mathbf{X}_{k-1}) = 1$ when $\hat{\mathbf{R}}_{\mathbf{x}_k, X_{k-1}} = 0$. It implies that when $\mathbf{x}_k$ is close to any former point $\mathbf{x}_i$ $(i < k)$, M is close to zero. Therefore, EI&MI will keep the infilled samples away from each other.

3.3 Multiple points infilling criterion: EIGD

As introduced in the last section, EI&MI was proposed to prevent the distance among points to be too close by maximizing

(a) GD function with $\rho = 0.3$
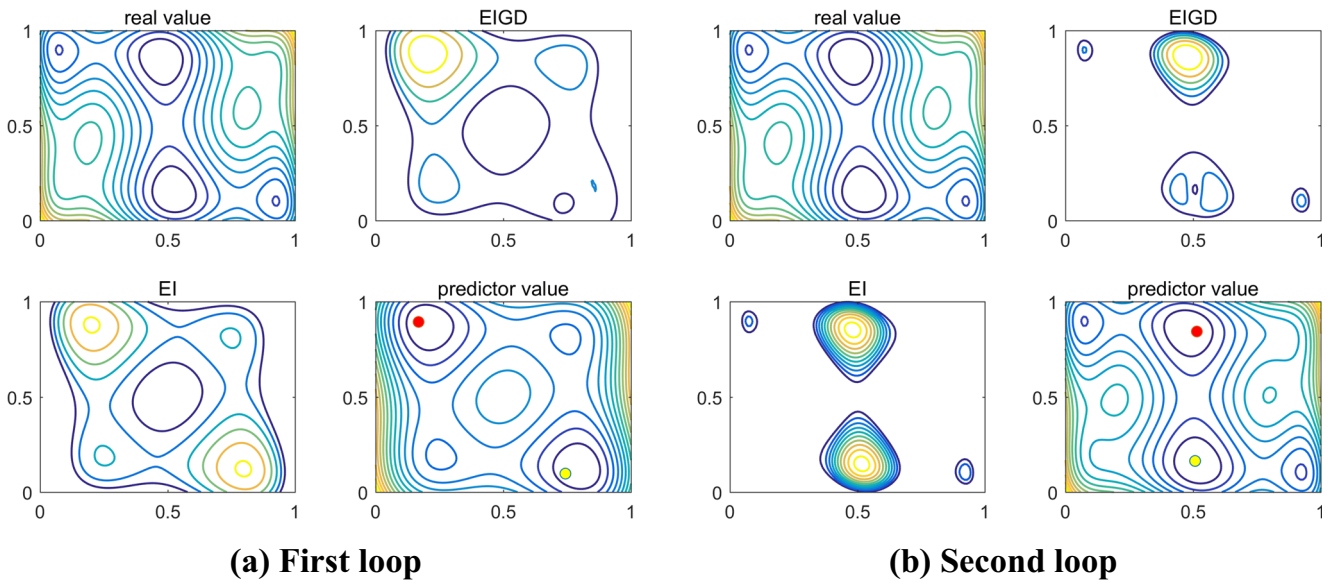

(b) GD function with $\alpha = 100$

Fig. 3 Updating loops of six-hump camel-back function with infilling points added by EIGD. **a** First loop **b** Second loop

the entropy principle. However, the expression of $M(\mathbf{x}_k, \mathbf{X}_{k-1})$ is so complicated that limits the applicability for engineering problems. In order to simplify the implementation process, a new multiple points infilling criterion named expected improvement with Gauss distance (EIGD) is developed in this section. The EIGD adopts the Gauss function to balance the distance among multiple points, and the implementation process can be greatly simplified. In addition, other kernel functions can also be used to keep the distance, as shown in Table 1.

In each updating loop, once surrogate model is established, EI will be known at any design space. When the first infilling point is obtained based on EI, the next point should be keep a distance away from its location. In view of this point, Gauss function can be adapted to describe the influence of the infilling points added.

Find $\mathbf{x}_k$

Maximize $EIGD(\mathbf{x}_k) = E[I(\mathbf{x}_k)] \left[\prod_{i=1}^{k-1} \left(1 - Gauss(\mathbf{x}_k, \mathbf{x}_i, \alpha)\right) \right]^{\rho}$

Subject to : $\mathbf{x}_k \in \Omega \quad k = 1, 2, \cdots, n$

$$(19)$$

where $\mathbf{x}_k$ is the kth infilling point, and k-1 points have been filled.
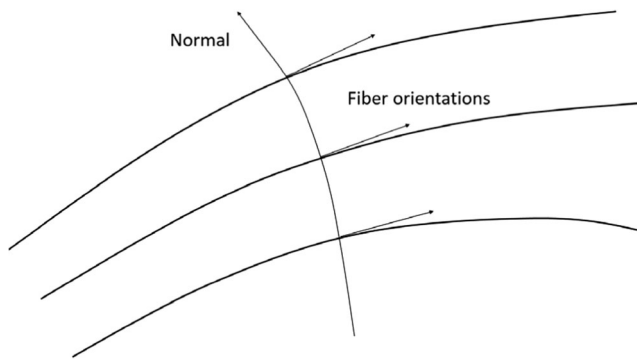

Fig. 4 Illustration of fiber parallelism

Herein, a benchmark mathematical problem (i.e. six-hump camel-back function shown as Fig. 1) is adapted to demonstrate the effectiveness of EIGD.

$$f(x) = \left(4 - 2.1x_1^2 + \frac{1}{3}x_1^4\right)x_1^2 + x_1 x_2$$
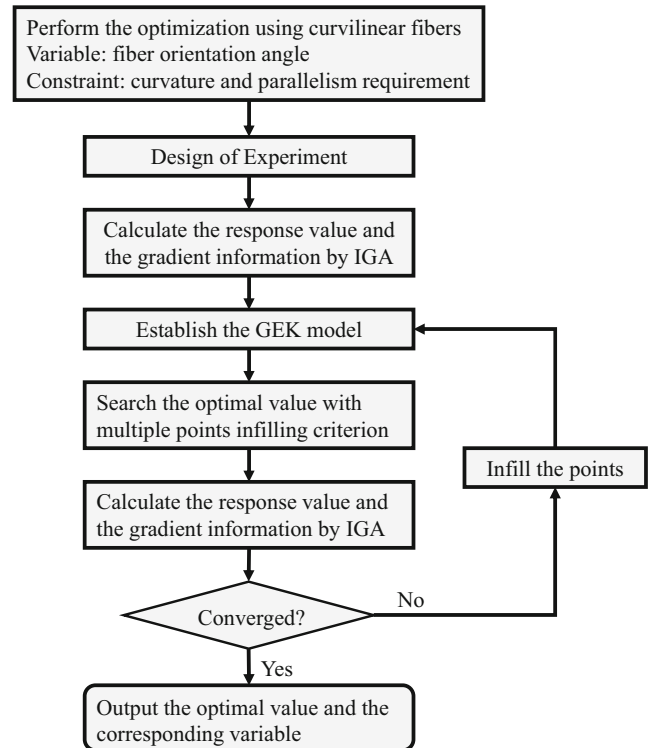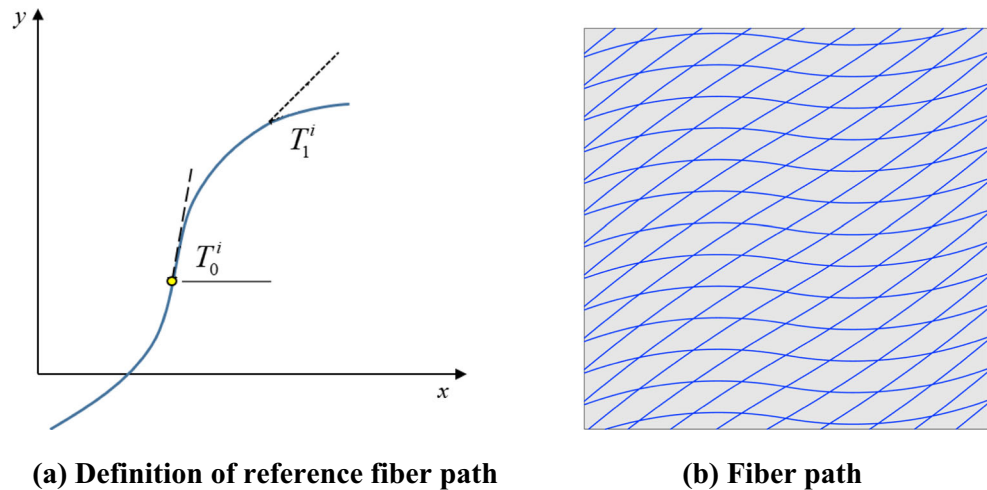$$+ \left(4x_2^2 - 4\right)x_2^2, x_1 \in [-2, 2], x_2 \in [-1, 1] \quad (20)$$

Fig. 5 The proposed optimization framework of variable-stiffness panels based on GEK

Fig. 6 Variable-stiffness panel based on linear variation function. (a) Definition of reference fiber path (b) Fiber path

(a) Definition of reference fiber path   **(b) Fiber path**

For this benchmark example, 9 original sample points are used to establish the GEK model, and two infilling points are added to the training set in each loop. The Gauss distance can be obtained when dimension is one as

$$GD = (1 - Gauss(\mathbf{x}_k, \mathbf{x}_i, \alpha))^\rho = \left(1 - \exp\left(-\alpha |d|^2\right)\right)^\rho \quad (21)$$

where d is the distance between $\mathbf{x}_k$ and $\mathbf{x}_i$, α and ρ are two parameters. In order to get the parameters rationally, the influences of α and ρ are investigated, as shown in Fig. 2. The value of GD should nearly be zero when the two points are near, and quickly to be one when the distance is large. As is evident from Fig. 2a and b, the red line meets the requirements. When α is more than 100 and ρ is less than 0.3, the GD function is steep. Similarly, when α is less than 100 and ρ is more than 0.3, the GD function is so flat that the area affected is too large. Thus, we set $\alpha = 100$, $\rho = 0.3$ in this study. The updating loops of six-hump camel-back function are shown in Fig. 3, in which the yellow point is the first one to add, and the red point is the second one. When the first point is to infill, EIGD equals to EI. When the second point is to infill, EIGD around the infilled points will times the coefficient of less than one, so the second point will away from the infilled points by searching the maximal EIGD. In this way, more than one peak can be found by EIGD criterion.

The proposed EIGD can control the distance among the infilling points in each loop, moreover, it is more convenient for implementation compared to EI&MI. Although EI&MI or EIGD can be used to add multiple points to find not only one local optimum, the computational cost of EIGD is much cheaper than that of EI&MI, especially when the number of infilling points is large.

4 Surrogate-based optimization framework of variable-stiffness panels considering manufacturing constraints

As already mentioned in the abstract, the Automated Tape Laying (ATL) and Automated Fiber Placement (AFP) technology allow the designer to find more flexible fiber path, which significantly increases the load-carrying potential and design space of composite components (Hao et al. 2016a). Also, it has been demonstrated that IGA can provide accuracy prediction of buckling factor with less computational cost compared to FEA method (Hao et al. 2017a). However, new types of constraints may be raised in the manufacturing process of variable-stiffness panels, and it should be considered in the design optimization to guarantee the manufacturability of the optimum design. In this section, two typical manufacturing constraints (Huang et al. 2016) are introduced for the AFP process, including curvature constraint and parallelism constraint.

Once the curvature of an innermost tow of a course becomes too severe, the compressed side would exhibit local buckling or wrinkle modes (Kahya 2016). For variable-stiffness panels, the curvature of fiber path at arbitrary point can be expressed as

$$cur(x, y) = \frac{|y''|}{\left|1 + y'^2\right|^{\frac{3}{2}}} \quad (22)$$
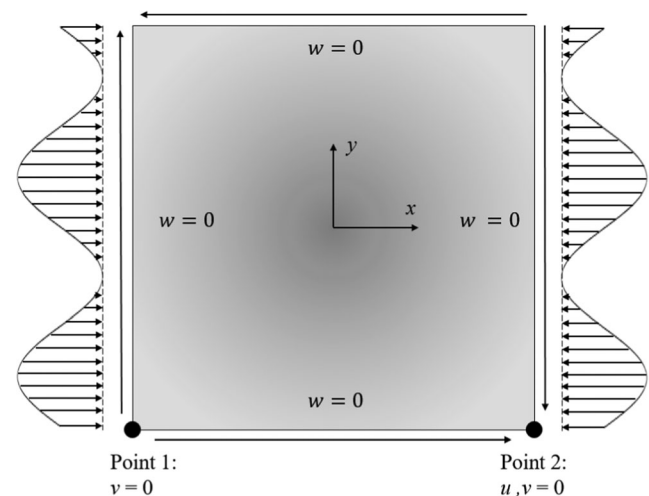

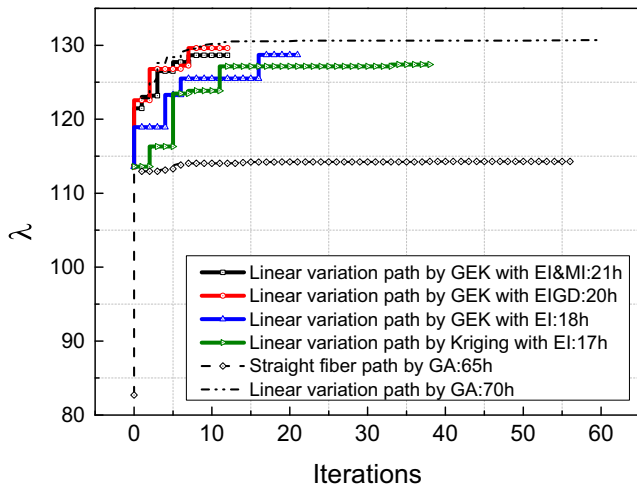**Fig. 7** Loading and boundary conditions of variable-stiffness panel

Fig. 8 Iterations histories of buckling factor by different optimizations

where y' is the derivative of y on x, and y'' is the derivative of y' on x.

To eliminate the phenomenon of gaps and overlaps, the fiber orientations along the normal should not change excessively, as shown in Fig. 4. The parallelism constraint is defined as

$$par(x,y) = \left| \frac{\partial \theta}{\partial \boldsymbol{n}} \right| \quad (23)$$

A surrogate-based optimization framework is proposed in Fig. 5, by which the advantages of IGA including exact modelling, analysis and analytical sensitivity can be fully utilized. Fiber orientation angles are

optimized with the objective of maximizing the buckling load. In the framework, various functions can be utilized to represent a family of curvilinear fiber path. The optimization problem can be formulated as

$$Maximize: \lambda$$

$$Subject\ to: \begin{cases} cur(x,y) \le c_m \\ par(x,y) \le p_m \\ X_i^l \le X_i \le X_i^u, i = 1,2,\cdots,n \\ (x,y) \in \Omega \end{cases} \quad (24)$$

where λ is the buckling factor, Ω is the design domain of the panel, c_m and p_m are the threshold values of fiber curvature and parallelism, X_i is the ith design variable to control the curvilinear fiber path, $X_i^l \le X_i \le X_i^u$, $i = 1$, $2, 3, 4$ and $X_i^l \le X_i \le X_i^u$, $i = 1, 2, 3, 4$ are the lower and upper bounds of the ith design variable. A set of sample points is generated in the process of design of experiment (DOE) to establish the surrogate model, e.g. Optimal Latin Hypercube Sample (OLHS). Due to the inherent feature of multimodal search problems, evolutionary algorithm (like Genetic Algorithm, GA) is used to find the optimum stacking sequence. In each updating loop, based on multiple infilling points criterions, several points that satisfy the constraints evaluated by IGA are added in each updating loop. If the convergence criterion is not satisfied, another new surrogate model will be built. Herein, the convergence criterion is set as: $EI < 10^{-4}$ and no improvement in three loops. For the proposed framework, both the global optimization capacity and optimization efficiency can be guaranteed.

Table 2 Optimum variable values of linear variation fiber path without manufacturing constraints

| Type	DOE	GEK			Kriging	GA	
		EI&MI	EIGD	EI	EI	Straight	Linear variation
T_0^1	3.690	56.735	54.619	29.399	11.741	43.942	49.231
T_1^1	47.790	47.317	47.185	53.149	50.923		43.975
T_0^2	55.080	44.865	35.122	75.803	56.433	45.794	49.032
T_1^2	42.210	44.115	44.957	40.719	43.972		44.828
T_0^3	53.280	89.765	7.565	87.098	55.203	44.659	9.096
T_1^3	44.100	47.340	51.251	44.759	47.425		51.392
T_0^4	90.000	0.058	8.111	0.231	76.630	40.914	2.327
T_1^4	53.280	56.458	49.595	55.690	42.469		51.445
T_0^5	0.000	6.712	85.828	1.564	5.877	30.788	89.773
T_1^5	14.670	55.434	42.379	56.759	49.977		40.947
λ	113.6	128.6	129.6	128.7	127.4	114.3	130.7
Iteration number	–	8	8	17	35	56	60
Improvement %	–	13.20	14.08	13.29	12.15	–	15.05
CPU time (h)	–	21	20	18	17	65	70
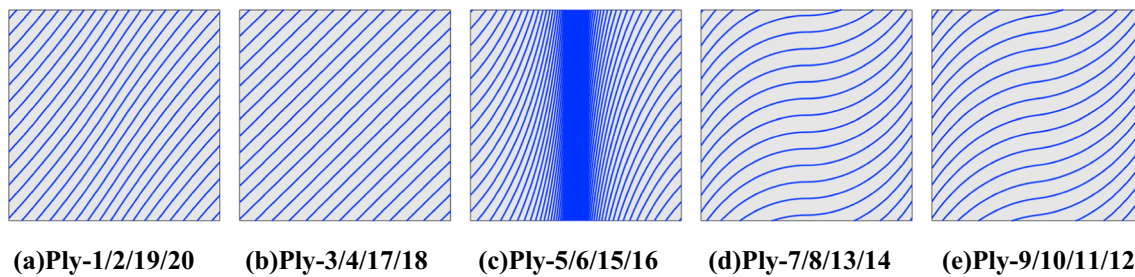
Fig. 9 Optimum fiber paths without manufacturing constraints (GEK-EI&MI). **a** Ply-1/2/19/20 **b** Ply-3/4/17/18 **c** Ply-5/6/15/16 **d** Ply-7/8/13/14 **e** Ply-9/10/11/12

5 Optimization of variable-stiffness panels with manufacturing constraints

5.1 Model description

For the linear variation path, the function of fiber orientation angle is along the x axis, which is assumed to be centered along the length l of the panel and can be defined as

$$\theta^i(x) = \frac{2\left(T_1^i - T_0^i\right)}{l}|x| + T_0^i \tag{25}$$

where T_0^i is the fiber orientation angle at the panel center of the ith layer, T_1^i is the fiber orientation angle at the panel boundary of the ith layer, $\theta^i(x)$ is the fiber orientation angle of the ith layer. The reference fiber path is shown in Fig. 6.

In the following sections, a square panel with a length of 254 mm is investigated. A 20-ply balanced symmetric laminate is used and the fiber angles of two adjacent plies are opposite. The lamina properties are set as $E_1 = 181.0$ GPa, $E_2 = 10.27$ GPa, $G_{12} = G_{13} = 7.17$ GPa, $G_{23} = 3.78$ GPa, $\upsilon_{12} = 0.28$, and the ply thickness is 0.15 mm.

5.2 Loading and boundary conditions

For aircraft panels, combined compression-shear load is a common design condition. Because the combined loading condition may cause complicated mode shapes with coupling pattern, complex loading path is required to increase the resistance to buckling. In this study, non-uniform loading is considered, and the amplitude of axial compression is $P = \sin(4\pi y/l + \pi/3)$, as shown in Fig. 7. This further highlights the load-carrying gain of variable-stiffness panels, which can tailor the in-plane stiffness by varying the fiber path. Besides, the boundary condition has a substantial influence on the buckling behavior and mode shape. A typical boundary condition (i.e. four loading edges simply supported, SSSS) is investigated in this study. The linear buckling analysis is performed based on IGA, and quadratic NURBS elements are used for IGA. Both the analysis procedure and sensitivity derivation are programed in MATLAB.

5.3 Optimization results

The proposed framework is used to conduct the optimization of variable-stiffness panels based on linear variation function, and the optimization formulations in each step can be found in Section 4. Due to the constraint of symmetric laminates, only 5 plies need to be designed. The involved design variables include the fiber orientation angle at the panel center and boundary. Therefore, a total number of 10 variables are involved in the optimization. The ranges of each variable are defined as follows

$$X_{i\cdot j} = T_j^i \in \left[0^\circ, 90^\circ\right], i = 1, 2, \cdots, 5, \ j = 1, 2 \tag{26}$$

We normalize the variables in the optimization, in order to guarantee the convergence rate of surrogate-based
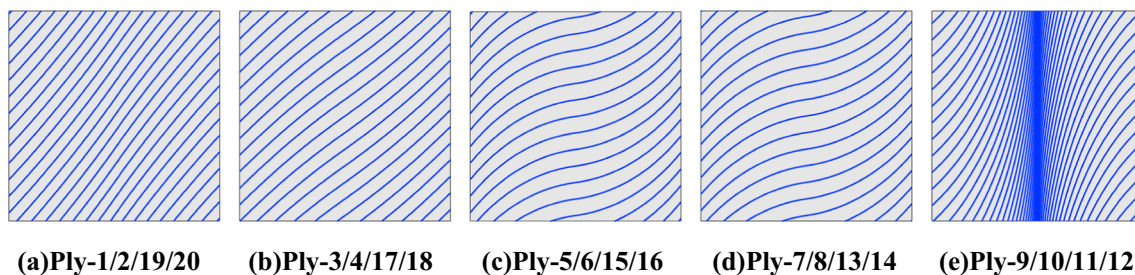

Fig. 10 Optimum fiber paths without manufacturing constraints (GEK-EIGD). **a** Ply-1/2/19/20 **b** Ply-3/4/17/18 **c** Ply-5/6/15/16 **d** Ply-7/8/13/14 **e** Ply-9/10/11/12
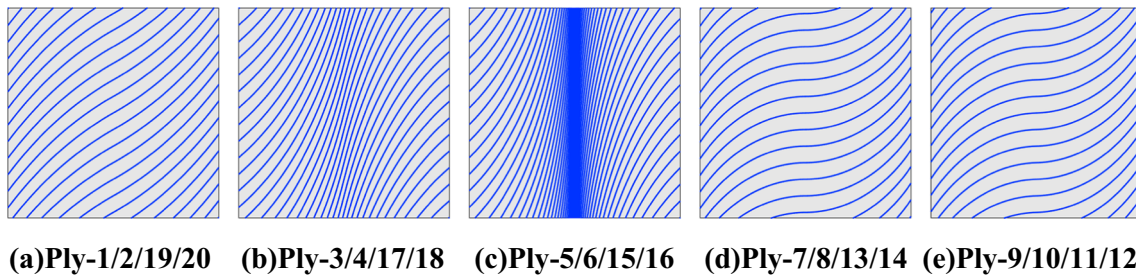
(a)Ply-1/2/19/20   (b)Ply-3/4/17/18   (c)Ply-5/6/15/16   (d)Ply-7/8/13/14   (e)Ply-9/10/11/12

Fig. 11 Optimum fiber paths without manufacturing constraints (GEK-EI). **a** Ply-1/2/19/20 **b** Ply-3/4/17/18 **c** Ply-5/6/15/16 **d** Ply-7/8/13/14 **e** Ply-9/10/11/12

optimization. Then, the buckling optimization of variable-stiffness panels is performed.

5.3.1 Optimization without manufacturing constraints

A set of 50 sample points is generated by the OLHS to establish the surrogate model firstly. In the updating process of surrogate model, several infilling criterions are compared, including EI&MI, EIGD and EI. For multiple infilling points criterions, 4 points evaluated by IGA are added in each updating loop. In the surrogate model method, genetic algorithm (GA) is used to search the maximum of EI or other infilling criterions. The algorithm parameters in GA are set as: population size = 200, max generations = 1000, crossover fraction = 0.8, mutation rate = 0.01, function tolerance = 10^{-6}. The iteration history is also shown in Fig. 8. The optimum values of design variables in each ply are listed in Table 2, where the column of DOE means the best result in Design of Experiment, and the row of improvement % means the percentage of improvement over DOE.

As is evident from Table 2, the number of required iterations for GEK with EI is much fewer than the original Kriging with EI. Moreover, the performance of optimum design by GEK is better, which demonstrates that the GEK method including gradient information is more efficient. Furthermore, comparing the infilling criterions based on GEK method, the EI&MI and EIGD criterions show higher computational efficiency than EI. Due to the fact that parallel computing method can be used in the multiple points infilling criterion, even if the number of

points is increased, the computational cost for infilling points remains almost unchanged, thus the GEK with EIGD criterion can be regarded as the most promising method.

To illustrate the computational efficiency and optimization capacity of proposed method, GA is also used to perform the global optimization directly (named as direct GA), and thus numerous function calls are involved in the optimization process. For this example, the total computational cost of direct GA is about 70 h, using a work station with a CPU of 2.20 Hz and 32G RAM, while the one is only 20 h for the optimization using GEK. The time of calculating buckling factor for each sample is about 20 s, and if the gradient information is required, the time will increase to 108 s. For direct GA, each population should be calculated by IGA, and about 20 s × 200 population × 60 iter ≈ 70 h. For GEK method, only 50 + 4 × 10 iter = 90 points need to be calculated by IGA, and the CPU time is about 90 × 108 s ÷ 4 parallel = 40 min. In each loop, the time to establish GEK is 24 min in average. And GA is used to search the maximum of EIGD, the time of calculating EIGD for one sample is about 22 min, and the total time will be 40 min + 24 min × 10 iter +22 min × 4 points × 10 iter ≈ 20 h, which is lower than the one based on EI&MI. Similarly, for Kriging method, the time cost on establishing model is 6 min in average, the time of calculating EI for one sample is about 20 min and the total time is 6 min × 38 iter +20 min × 38 iter ≈ 17 h.

In addition, Figs. 9, 10, 11, and 12 show the optimum fiber paths without manufacturing constraints for different methods. As is evident, the phenomenon of fiber enrichment can be found, and thus manufacturing constraints should be considered during
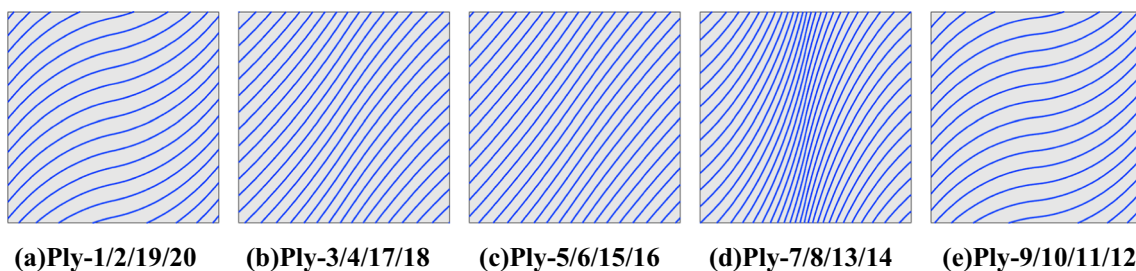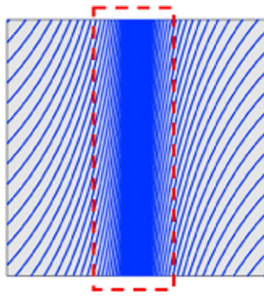

(a)Ply-1/2/19/20   (b)Ply-3/4/17/18   (c)Ply-5/6/15/16   (d)Ply-7/8/13/14   (e)Ply-9/10/11/12

Fig. 12 Optimum fiber paths without manufacturing constraints (Kriging-EI). (a)Ply-1/2/19/20 **b** Ply-3/4/17/18 **c** Ply-5/6/15/16 **d** Ply-7/8/13/14 **e** Ply-9/10/11/12

Fig. 13 Optimum linear variation function path without manufacturing constraints

the optimization process. After the optimization by GEK with EIGD, the buckling factor λ of curvilinear fiber path without manufacturing constraints increases from 113.6 to 129.6, with an improvement of 14.08%.

5.3.2 Optimization considering manufacturing constraints

In the above optimization, it is found that the linear variation fiber path is more flexible, and results indicate that the load-carrying capacity of variable-stiffness panel can be remarkably improved. However, the phenomenon of fiber enrichment can be found in the optimum design. For example, when the fiber orientation angle at the panel center or at the boundary of panel is close to $\pi/2$ or the change of local fiber angle is too sharp, the phenomenon of fiber enrichment can be found, as shown in Fig. 13, which greatly challenges the existing manufacturing technologies such as ATL and AFP.

In order to satisfy the practical manufacturing requirements, the fiber curvature constraint and parallelism constraint are introduced as typical manufacturing constraints during the optimi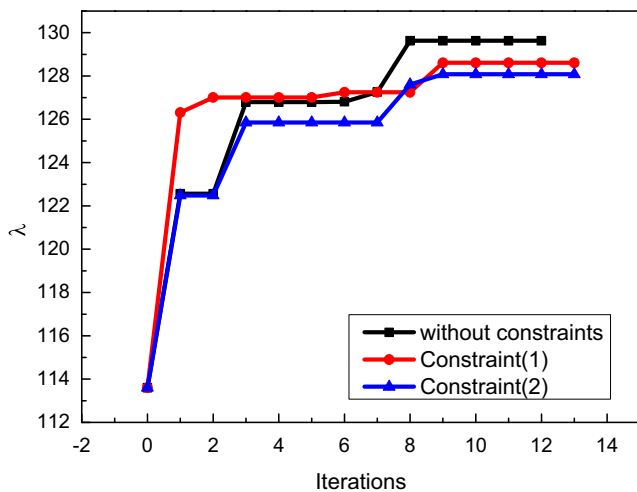zation process (Huang et al. 2016). In this study, the upper limit of fiber curvature c_m is set to be 0.1, and the parallelism p_m is set to be $\pi/6$ for Constraint (1) and $\pi/30$ for Constraint (2), respectively. For the linear variation function, the value of y coordination of the ith layer can be calculated from the fiber path function.

$$y^i(x) = \frac{l}{2(T_1^i - T_0^i)} \left\{ -\ln\left[\cos\left(T_0^i + \frac{2(T_1^i - T_0^i)}{l}|x|\right)\right] + \ln\left[\cos(T_0^i)\right] \right\}$$

$$(27)$$

And the curvature function can be written as:

$$cur(x, y^i) = \frac{|y^{i''}|}{|1 + y^{i'2}|^{\frac{3}{2}}} = \left|\frac{2(T_1^i - T_0^i)}{l}\cos(\phi_x^i)\right| \leq c_m$$

$$\Rightarrow |\cos(\phi_x^i)| \leq \left|\frac{l}{2(T_1^i - T_0^i)}\right| c_m$$

$$(28)$$

where, $\phi_x^i = T_0^i + \frac{2(T_1^i - T_0^i)}{l}|x|$ is the fiber orientation angle of the ith layer. For the linear variation path function, the curvature constraint is usually satisfied, when the panel size is not too small.

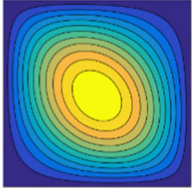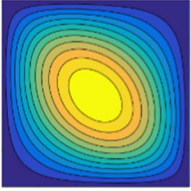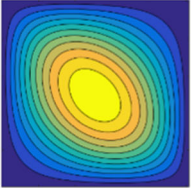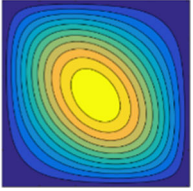Similarly, the parallelism function can be expressed as

$$par(x, y^i) = \left|\frac{\partial\theta}{\partial\boldsymbol{n}}\right| = \left|\frac{\partial\theta}{\partial x}n_1 + \frac{\partial\theta}{\partial y^i}n_2\right|$$

$$= \left|\frac{4(T_1^i - T_0^i)}{l \cdot \cos(\phi_x^i)\tan(2\phi_x^i)}\right| \leq p_m$$

$$(29)$$

Note that (29) achieves the maximal value when ϕ_x^i is close to 0 or $\pi/2$, which means that the maximum par can only appear at the center of the panel or the

Fig. 14 Iteration histories of buckling factor for linear variation fiber paths by using GEK with EIGD

Table 3 Optimum variable values of linear variation fiber path considering/without manufacturing constraints

Type	DOE	Without manufacturing constraints	Considering manufacturing constraints	
p_m	–	–	$\pi/6$	$\pi/30$
T_0^1	3.690	54.619	42.622	63.856
T_1^1	47.790	47.185	46.612	42.182
T_0^2	55.080	35.122	70.821	69.072
T_1^2	42.210	44.957	47.195	47.358
T_0^3	53.280	7.565	1.005	7.084
T_1^3	44.100	51.251	49.562	56.572
T_0^4	90.000	8.111	1.008	3.038
T_1^4	53.280	49.595	53.022	55.414
T_0^5	0.000	85.828	83.542	20.177
T_1^5	14.670	42.379	41.591	48.662
λ	113.6	129.6	128.6	128.1
Iteration number	–	8	9	9
Improvement %	–	14.08	13.20	12.76

Table 4 Buckling modes of different optimum designs based on straight and linear variation fiber paths

Mode order	Straight fiber path	Linear variation fiber path		
---	---	Without manufacturing constraints	Constraint (1)	Constraint (2)
①				
	λ =114.3	λ =129.6	λ =128.6	λ =128.1

boundary of the panel. Therefore, an easy way to avoid the condition of $par(x, y^j) > p_m$ is to limit the range of fiber variation. On this basis, the optimization of curvilinear fiber path is carried out based on GEK with EIGD. Taking the SSSS boundary condition for example, the iteration history of buckling factor λ is shown in Fig. 14. The optimum values of design variables are listed in Table 3, and the buckling modes are listed in Table 4.

When the Constraint (1) is taken into account, the buckling factor λ of curvilinear fiber path increases from 113.6 to 128.6, with an improvement of 13.20%. And for the Constraint (2), the constraint is tighter, and thus the buckling factor λ only increases to 128.1, with an improvement of 12.76%.

To further investigate the influence of manufacturing constraints, the optimum fiber paths considering curvature constraint and parallelism constraint are shown in Figs. 15 and 16. As can be observed, the constraint is not active for Constraint (1), thus the fiber enrichment occurs. Instead, when the constraint is tightened for Constraint (2), the fiber enrichment is well eliminated, and the curvilinear fiber path becomes smooth. In general, the arrangement of fiber satisfies the requirement of stiffness distribution to avoid stress concentration. This will allow for a better understanding of load redistribution mechanism, which can be responsible for a significantly increased buckling load. Moreover, the AFP technology is adequate for manufacturing this type of composite panels, and this can be attributed to the curvature constraint and parallelism constraint.

Besides, in order to illustrate the excellent performance of curve fiber, the optimization of straight fiber is also compared. For straight fiber, the stacking sequence of initial design is [±0°, ±22.5°, ±45°, ±67.5°, ±90°, ±90°, ±67.5°, ±45°, ±22.5°, ±0°]$_s$. After

(a)Ply-1/2/19/20   **(b)Ply-3/4/17/18**   **(c)Ply-5/6/15/16**   **(c)Ply-7/8/13/14**   **(d)Ply-9/10/11/12**
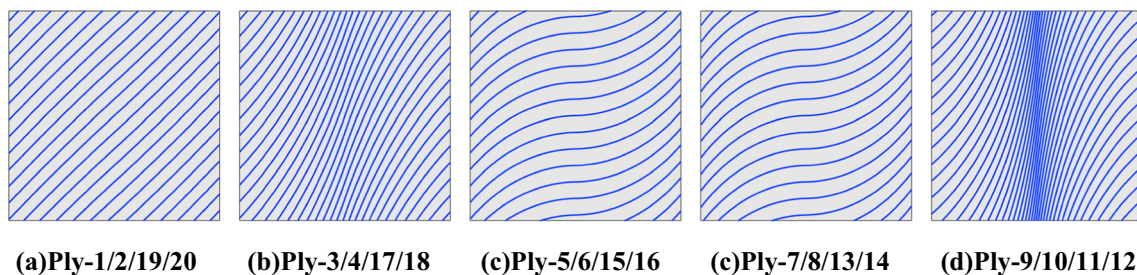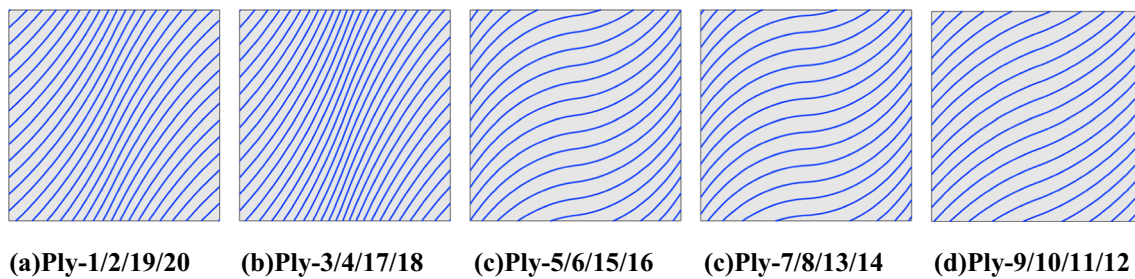
Fig. 15 Optimum fiber paths with manufacturing constraint (1) (GEK-EIGD). **a** Ply-1/2/19/20 **b** Ply-3/4/17/18 **c** Ply-5/6/15/16 **d** Ply-7/8/13/14 **e** Ply-9/10/11/12

(a)Ply-1/2/19/20   **(b)Ply-3/4/17/18**   **(c)Ply-5/6/15/16**   **(c)Ply-7/8/13/14**   **(d)Ply-9/10/11/12**

Fig. 16 Optimum fiber paths with manufacturing constraint (2) (GEK-EIGD). **a** Ply-1/2/19/20 **b** Ply-3/4/17/18 **c** Ply-5/6/15/16 **d** Ply-7/8/13/14 **e** Ply-9/10/11/12

performing linear buckling analysis, the buckling factor λ is obtained as 82.7 for the SSSS boundary condition. Then, GA is adopted to perform the optimization. The iteration history of buckling factor is shown in Fig. 8. After 56 iterations, the optimum buckling factor λ of panel is 114.3, with an improvement of 38.2%. By comparing the optimum designs of straight fiber path and curvilinear fiber path, the buckling factor increases from 114.3 to 130.7 for the curvilinear fiber path, with an improvement of 14.35%.

6 Conclusions

In this paper, an efficient optimization framework is developed for the design of variable-stiffness panels by combination of IGA method, GEK method and multiple points infilling criterion, where IGA can provide analytical gradient information and accuracy prediction of buckling factor with less computational cost compared to FEA method, moreover, GEK can use the gradient information to improve the accuracy of surrogate model. These characteristics make the combination of IGA and GEK become an efficient method. Furthermore, on the basis of EI&MI criterion, a new multiple points infilling criterion named EIGD is developed, which can enhance the global optimization capacity of GEK and simplify the implementation of EI&MI.

A square panel with linear variation fiber path is served as illustrative example. The performance of proposed method is compared with original Kriging, GEK with EI, GEK with EI&MI. The fiber paths and buckling modes as well as buckling factors of the optimum designs are examined in detail. It can be found that the GEK exhibits better performance than original Kriging method in terms of both global optimization capacity and computational efficiency. Moreover, using multiple points infilling criterion can further increase the optimization efficiency of EI infilling

criterion, and the computing cost of EIGD in each iteration is cheaper than EI&MI. Besides, the effects of manufacturing constraints are investigated. It can be concluded that the phenomenon of fiber enrichment can be well eliminated by an appropriate selection of curvature constraint and parallelism constraint. In summary, the combination of GEK, IGA and EIGD is a promising optimization framework, which can significantly improve the load-carrying efficiency of variable-stiffness panels for future aerospace and aircraft industries.

Appendix

The predicted function of GEK can be written as

$$\hat{y}(x) = \sum_{i=1}^{n} \omega_i y_i + \sum_{i=0}^{n} \sum_{j=0}^{d} \nu_j^i \frac{\partial y(\boldsymbol{x}^i)}{\partial x_j^i} \qquad (30)$$

where ω_i denotes the weight coefficient of the ith response value, and ν_j^i denotes the weight coefficient the partial derivative of the jth dimensional design variable to the ith response value. The regression function is defined as

$$\begin{aligned}
&Cov\big(Z(\boldsymbol{x}^i), Z(\boldsymbol{x}^j)\big) = \sigma^2 R(\boldsymbol{x}^i, \boldsymbol{x}^j) \\
&Cov\bigg(Z(\boldsymbol{x}^i), \frac{\partial Z(\boldsymbol{x}^j)}{\partial \boldsymbol{x}_k}\bigg) = \sigma^2 \frac{\partial R(\boldsymbol{x}^i, \boldsymbol{x}^j)}{\partial x_k^j} = -Cov\bigg(\frac{\partial Z(\boldsymbol{x}^i)}{\partial \boldsymbol{x}_k}, Z(\boldsymbol{x}^j)\bigg) \\
&Cov\bigg(\frac{\partial Z(\boldsymbol{x}^i)}{\partial \boldsymbol{x}_k}, \frac{\partial Z(\boldsymbol{x}^j)}{\partial \boldsymbol{x}_l}\bigg) = \sigma^2 \frac{\partial^2 R(\boldsymbol{x}^i, \boldsymbol{x}^j)}{\partial x_k^i \partial x_l^j}
\end{aligned} \qquad (31)$$

So far, the weight coefficients can be calculated by solving the minimization problem about $MSE(\boldsymbol{x})$ with

the Lagrange multiplier approach. It can be found as follows

$$
\begin{cases}
\sum_{j=1}^{n} \omega_j Cov\big(Z(\pmb{x}^i), Z(\pmb{x}^j)\big) + \sum_{j=1}^{n} \nu_i^j Cov\bigg(Z(\pmb{x}^i), \frac{\partial Z(\pmb{x}^j)}{\partial x_k}\bigg) + \frac{\mu}{2} = Cov\big(Z(\pmb{x}^i), Z(\pmb{x})\big), i = 1, 2 \cdots, n \\
\sum_{j=1}^{n} \omega_j Cov\bigg(\frac{\partial Z(\pmb{x}^i)}{\partial x_k}, Z(\pmb{x}^j)\bigg) + \sum_{j=1}^{n} \nu_i^j Cov\bigg(\frac{\partial Z(\pmb{x}^i)}{\partial x_k}, \frac{\partial Z(\pmb{x}^j)}{\partial x_l}\bigg) = Cov\bigg(\frac{\partial Z(\pmb{x}^i)}{\partial x_k}, Z(\pmb{x})\bigg), i = 1, 2 \cdots, n \\
\sum_{i=0}^{n} \omega_i = 1
\end{cases}
\tag{32}
$$

And μ is the Lagrange multipliers.

Also, (35) can be written as a matrix function

$$
\begin{bmatrix} \pmb{R} & \pmb{F} \\ \pmb{F}^T & 0 \end{bmatrix} \begin{bmatrix} \pmb{\nu} \\ \tilde{\mu} \end{bmatrix} = \begin{bmatrix} \pmb{r}_{(x)} \\ 1 \end{bmatrix}
\tag{33}
$$

where

$$
\tilde{\mu} = -\frac{\mu}{2\sigma^2} = \big(\pmb{F}^T \pmb{R}^{-1} \pmb{F}\big)^{-1} \big(\pmb{F}^T \pmb{R}^{-1} \pmb{r}_{(x)} - 1\big)
$$
$$
\pmb{F} = [1, \cdots, 1, 0, 0, \cdots, 0]^T \in \mathfrak{R}^{n+n \times dim}
$$
$$
\pmb{\nu} = \big[\omega_1, \cdots, \omega_n, \nu_1^1, \nu_2^1, \cdots, \nu_{dim}^n\big]^T = \pmb{R}^{-1} \big(\pmb{r}_{(x)} - F \tilde{\mu}\big)
$$

The correlation vector and the correlation matrix can be expressed as

$$
\pmb{r}_{(x)} = \bigg[\pmb{R}(\pmb{x}, \pmb{x}^1) \cdots \pmb{R}(\pmb{x}, \pmb{x}^n), \frac{\partial R(\pmb{x}, \pmb{x}^1)}{\partial x_1^1}, \frac{\partial R(\pmb{x}, \pmb{x}^1)}{\partial x_2^1}, \cdots, \frac{\partial R(\pmb{x}, \pmb{x}^1)}{\partial x_{dim}^1}, \cdots \frac{\partial R(\pmb{x}, \pmb{x}^n)}{\partial x_{dim}^n} \bigg]^T \in \mathfrak{R}^{n+ndim}
$$

$$
\pmb{R} = \begin{bmatrix}
R(\pmb{x}^1, \pmb{x}^1) & \cdots & R(\pmb{x}^1, \pmb{x}^n) & \dfrac{\partial R(\pmb{x}^1, \pmb{x}^1)}{\partial x_1^1} & \dfrac{\partial R(\pmb{x}^1, \pmb{x}^1)}{\partial x_2^1} & \cdots & \dfrac{\partial R(\pmb{x}^1, \pmb{x}^n)}{\partial x_{dim}^n} \\
\vdots & \ddots & \vdots & \vdots & \vdots & \ddots & \vdots \\
R(\pmb{x}^n, \pmb{x}^1) & \cdots & R(\pmb{x}^n, \pmb{x}^n) & \dfrac{\partial R(\pmb{x}^n, \pmb{x}^1)}{\partial x_1^1} & \dfrac{\partial R(\pmb{x}^n, \pmb{x}^1)}{\partial x_2^1} & \cdots & \dfrac{\partial R(\pmb{x}^n, \pmb{x}^n)}{\partial x_{dim}^n} \\
\dfrac{\partial R(\pmb{x}^1, \pmb{x}^1)}{\partial x_1^1} & \cdots & \dfrac{\partial R(\pmb{x}^n, \pmb{x}^1)}{\partial x_1^1} & \dfrac{\partial^2 R(\pmb{x}^1, \pmb{x}^1)}{\partial x_1^1 \partial x_1^1} & \dfrac{\partial^2 R(\pmb{x}^1, \pmb{x}^1)}{\partial x_1^1 \partial x_2^1} & \cdots & \dfrac{\partial^2 R(\pmb{x}^1, \pmb{x}^n)}{\partial x_1^1 \partial x_{dim}^n} \\
\dfrac{\partial R(\pmb{x}^1, \pmb{x}^1)}{\partial x_2^1} & \cdots & \dfrac{\partial R(\pmb{x}^n, \pmb{x}^1)}{\partial x_2^1} & \dfrac{\partial^2 R(\pmb{x}^1, \pmb{x}^1)}{\partial x_2^1 \partial x_1^1} & \dfrac{\partial^2 R(\pmb{x}^1, \pmb{x}^1)}{\partial x_2^1 \partial x_2^1} & \cdots & \dfrac{\partial^2 R(\pmb{x}^1, \pmb{x}^n)}{\partial x_2^1 \partial x_{dim}^n} \\
\vdots & \ddots & \vdots & \vdots & \vdots & \ddots & \vdots \\
\dfrac{\partial R(\pmb{x}^1, \pmb{x}^n)}{\partial x_{dim}^n} & \cdots & \dfrac{\partial R(\pmb{x}^n, \pmb{x}^n)}{\partial x_{dim}^n} & \dfrac{\partial^2 R(\pmb{x}^1, \pmb{x}^n)}{\partial x_{dim}^n \partial x_1^1} & \dfrac{\partial^2 R(\pmb{x}^1, \pmb{x}^n)}{\partial x_{dim}^n \partial x_2^1} & \cdots & \dfrac{\partial^2 R(\pmb{x}^n, \pmb{x}^n)}{\partial x_{dim}^n \partial x_{dim}^n}
\end{bmatrix} \in \mathfrak{R}^{(n+ndim) \times (n+ndim)}
\tag{34}
$$

The predicted *MSE* of $\hat{y}(x)$ is

$$
s_{(x)}^2 = \sigma^2 \Big(1 + \big(\pmb{F}^T \pmb{R}^{-1} \pmb{F}\big)^{-1} \big(1 - \pmb{F}^T \pmb{R}^{-1} \pmb{r}_{(x)}\big)^2 - r_{(x)}^T \pmb{R}^{-1} \pmb{r}_{(x)} \Big)
\tag{35}
$$

As both $\hat{y}(x)$ and *MSE* are the functions of σ^2 and θ, θ can be calculated by the maximum likelihood estimation approach. $\hat{y}(x)$ follows the multidimensional normal distribution as

$$
P\big(Y(\pmb{x})|\pmb{\theta}, \sigma^2, \hat{y}(\pmb{x})\big) = L\big(\pmb{\theta}, \sigma^2|\hat{y}(\pmb{x}) = Y(\pmb{x})\big)
$$
$$
= \frac{1}{(2\pi\sigma^2)^{\frac{n(1+dim)}{2}} |\pmb{R}|^{\frac{1}{2}}} \exp\left[-\frac{(\pmb{Y} - \beta \pmb{F})^T \pmb{R}^{-1}(\pmb{Y} - \beta \pmb{F})}{2\sigma^2} \right]
$$
$$
\ln\big(L(\pmb{\theta}, \sigma^2, \hat{y}(\pmb{x})|Y(\pmb{x}))\big) = -\frac{n(1+dim)}{2} \ln(2\pi) - \frac{n(1+dim)}{2} \ln(\sigma^2) - \frac{1}{2} \ln|\pmb{R}| - \frac{(\pmb{Y} - \beta \pmb{F})^T \pmb{R}^{-1}(\pmb{Y} - \beta \pmb{F})}{2\sigma^2}
\tag{36}
$$

Take the partial derivative with respect to σ^2 of this equation and let it zero, σ^2 and β can be obtained as

$$\sigma^2 = \frac{1}{n(1+dim)}(Y-\beta F)^T R^{-1}(Y-\beta F)$$

$$\beta = (F^T R^{-1} F)^{-1} F^T R^{-1} Y \tag{37}$$

References

Abouhamze M, Shakeri M (2007) Multi-objective stacking sequence optimization of laminated cylindrical panels using a genetic algorithm and neural networks. Compos Struct 81(2):253–263

Blom AW, Tatting BF, Hol JMAM (2009) Fiber path definitions for elastically tailored conical shells. Compos Part B Eng 40(1):77–84

Bourada F, Amara K, Tounsi A (2016) Buckling analysis of isotropic and orthotropic plates using a novel four variable refined plate theory. Steel Compos Struct 21(6):1287–1306

Brampton CJ, Wu KC, Kim HA (2015) New optimization method for steered fiber composites using the level set method. Struct Multidiscip O 52(3):493–505

Chung HS, Alonso J (2002) Using gradients to construct cokriging approximation models for high-dimensional design optimization problems. AIAA paper 317:2002

Gürdal Z, Tatting BF, Wu CK (2008) Variable stiffness composite panels: effects of stiffness variation on the in-plane and buckling response. Compos Part A-Appl S 39(5):911–922

Haftka RT, Villanueva D, Chaudhuri A (2016) Parallel surrogate-assisted global optimization with expensive functions–a survey. Struct Multidiscip O 54(1):3–13

Han ZH, Görtz S (2012) Hierarchical kriging model for variable-fidelity surrogate modeling. AIAA J 50(9):1885–1896

Hao P, Wang B, Li G (2012) Surrogate-based optimum design for stiffened shells with adaptive sampling. AIAA J 50(11):2389–2407

Hao P, Wang B, Li G, Tian K, Du KF, Wang XJ, Tang XH (2013) Surrogate-based optimization of stiffened shells including load-carrying capacity and imperfection sensitivity. Thin-Walled Struct 72(15):164–174

Hao P, Wang B, Tian K, Li G, Zhang X (2016a) Optimization of curvilinearly stiffened panels with single cutout concerning the collapse load. Int J Struct Stab Dy 16:1550036–1–1550036–21

Hao P, Wang B, Du KF, Li G, Tian K, Sun Y, Ma YL (2016b) Imperfection-insensitive design of stiffened conical shells based on perturbation load approach. Compos Struct 136:405–413

Hao P, Yuan XJ, Liu HL, Wang B, Liu C, Yang DX, Zhan SX (2017a) Isogeometric buckling analysis of composite variable-stiffness panels. Compos Struct 165:192–208

Hao P, Wang YT, Liu C, Wang B (2017b) A novel non-probabilistic reliability-based design optimization algorithm using enhanced chaos control method. Comput Method Appl M 318:572–593

Huang D, Allen TT, Notz WI (2006) Global optimization of stochastic black-box systems via sequential kriging meta-models. J Glob Optim 34(3):441–466

Huang G, Wang H, Li G (2016) An efficient reanalysis assisted optimization for variable-stiffness composite design by using path functions. Compos Struct 153:409–420

Hughes TJR, Cottrell JA, Bazilevs Y (2005) Isogeometric analysis: CAD, finite elements, NURBS, exact geometry and mesh refinement. Comput Methods Appl Mech Eng 194(39):4135–4195

Jing Z, Fan XL, Sun Q (2015) Global shared-layer blending method for stacking sequence optimization design and blending of composite structures. Compos B: Eng 69:181–190

Jing Z, Sun Q, Silberschmidt VV (2016) A framework for design and optimization of tapered composite structures part I: from individual panel to global blending structure. Compos Struct 154:106–128

Jones DR, Schonlau M, Welch WJ (1998) Efficient global optimization of expensive black-box functions. J Glob Optim 13(4):455–492

Kahya V (2016) Buckling analysis of laminated composite and sandwich beams by the finite element method. Compos Part B Eng 91:126–134

Karakaya Ş, Soykasap Ö (2009) Buckling optimization of laminated composite plates using genetic algorithm and generalized pattern search algorithm. Struct Multidiscip O 39(5):477–486

Kristinsdottir BP, Zabinsky ZB, Tuttle ME (2001) Optimal design of large composite panels with varying loads. Compos Struct 51(1):93–102

Laurenceau J, Sagaut P (2008) Building efficient response surfaces of aerodynamic functions with kriging and cokriging. AIAA J 46(2):498

Laurent L, Boucard PA, Soulier B (2013) Generation of a cokriging metamodel using a multiparametric strategy. Comput Mech 51(2):151–169

Le Riche R, Haftka RT (1993) Optimization of laminate stacking sequence for buckling load maximization by genetic algorithm. AIAA J 31(5):951–956

Li Z, Ruan S, Gu J (2016) Investigation on parallel algorithms in efficient global optimization based on multiple points infill criterion and domain decomposition. Struct Multidiscip O 54(4):747–773

Liu W, Batill SM (2002) Gradient-enhanced response surface approximations using kriging models. AIAA/ISSMO S EXH M: 4–6

Liu B, Haftka RT, Akgün MA (2000) Permutation genetic algorithm for stacking sequence design of composite laminates. Comput Method Appl M 186(2):357–372

Liu D, Toropov VV, Querin OM (2011) Bilevel optimization of blended composite wing panels. J Aircr 48(1):107

Lozano GG, Tiwari A, Turner C (2016) A review on design for manufacture of variable stiffness composite laminates. P I Mech Eng B 230(6):981–992

Madeo A, Groh RMJ, Zucco G (2017) Post-buckling analysis of variable-angle tow composite plates using Koiter's approach and the finite element method. Thin-Walled Struct 110:1–13

Montemurro M, Catapano A (2017) On the effective integration of manufacturability constraints within the multi-scale methodology for designing variable angle-tow laminates. Compos Struct 161:145–159

Morris MD, Mitchell TJ, Ylvisaker D (1993) Bayesian design and analysis of computer experiments: use of derivatives in surface prediction. Technometrics 35(3):243–255

Muc A, Ulatowska A (2010) Design of plates with curved fiber format. Compos Struct 92(7):1728–1733

Nik MA, Fayazbakhsh K, Pasini D (2014) A comparative study of metamodeling methods for the design optimization of variable stiffness composites. Compos Struct 107:494–501

Niu XJ, Yang T, Du Y (2016) Tensile properties of variable stiffness composite laminates with circular holes based on potential flow functions. Arch Appl Mech 86(9):1551–1563

Peeters DMJ, Hesse S, Abdalla MM (2015) Stacking sequence optimisation of variable stiffness laminates with manufacturing constraints. Compos Struct 125:596–604

Rehman SU, Langelaar M, Keulen FV (2014) Efficient kriging-based robust optimization of unconstrained problems. J Comput Sci 5(6):872–881

Rikards R, Abramovich H, Auzins J (2004) Surrogate models for optimum design of stiffened composite shells. Compos Struct 63(2):243–251

Rouhi M, Ghayoor H, Hoa SV (2017) Computational efficiency and accuracy of multi-step design optimization method for variable stiffness composite structures. Thin-Walled Struct 113:136–143

Sasena MJ, Papalambros P, Goovaerts P (2002) Exploration of metamodeling sampling criteria for constrained global optimization. Eng Optim 34(3):263–278

Sóbester A, Leary SJ, Keane AJ (2005) On the design of optimization strategies based on global response surface approximation models. J Glob Optim 33(1):31–59

Soremekun G, Gürdal Z, Haftka RT (2001) Composite laminate design optimization by genetic algorithm with generalized elitist selection. Comput Struct 79(2):131–143

Sørensen SN, Lund E (2013) Topology and thickness optimization of laminated composites including manufacturing constraints. Struct Multidiscip O 48(2):249–265

Todoroki A, Sekishiro M (2008) Modified efficient global optimization for a hat-stiffened composite panel with buckling constraint. AIAA J 46(9):2257

Ulaganathan S, Couckuyt I, Ferranti F (2015) Performance study of multi-fidelity gradient enhanced kriging. Struct Multidiscip O 51(5):1017–1033

Van den Brink WM, Vankan WJ, Maas R (2012) Buckling optimized variable stiffness laminates for a composite fuselage window section. Int C Aer SCI B

Viana FAC, Haftka RT, Watson LT (2013) Efficient global optimization algorithm assisted by multiple surrogate techniques. J Glob Optim 56(2):669–689

Wang P, Costin DP (1992) Optimum design of a composite structure with three types of manufacturing constraints. AIAA J 30(6):1667–1669

Wang K, Kelly D, Dutton S (2002) Multi-objective optimisation of composite aerospace structures. Compout Struct 57(1):141–148

Wang B, Hao P, Li G et al (2014) Two-stage size-layout optimization of axially compressed stiffened panels. Struct Multidiscip O 50(2):313–327

Wu Z, Raju G, Weaver PM (2015) Framework for the buckling optimization of variable-angle tow composite plates. AIAA J 53(12):3788–3804

Yamazaki W, Mavriplis DJ (2013) Derivative-enhanced variable fidelity surrogate modeling for aerodynamic functions. AIAA J 51(1):126–137

Yamazaki W, Rumpfkeil MP, Mavriplis DJ (2010) Design optimization utilizing gradient/hessian enhanced surrogate model. 20104363 AIAA

Zehnder N, Ermanni P (2006) A methodology for the global optimization of laminated composite structures. Compos Struct 72(3):311–320

Zhu JH, Zhang WH, Xia L (2016) Topology optimization in aircraft and aerospace structures design. Arch Comput Method E 23(4):595–622